Int. J. Heat Mass Transfer. Vol. 11, pp. 1087–1104. Pergamon Press 1968. Printed in Great Britain

HEAT TRANSFER AND PRESSURE DROP IN HORIZONTAL ANNULAR TWO-PHASE, TWO-COMPONENT FLOW

R. H. PLETCHER* and H. N. McMANUS, Jr.†

(*Received* 26 *June* 1967 *and in revised form* 15 *December* 1967)

Abstract—The static pressure drop and both the local and average heat-transfer coefficients were measured for the horizontal annular flow of water and air in a tube with an I.D. of 1 in. The electrically heated stainless steel heat-transfer section 60 in long was located approximately 105 in downstream of liquid injection. Tube wall temperatures were measured by fifty-seven buried and twenty-two surface thermocouples. The water flow rate varied from 0·0714 to 0·3836 lb/s; the air flow rate, from 0·0300 to 0·2573 lb/s; and the heat flux, from 7372 to 12772 Btu/h ft^2. Sizeable circumferential variations in tube wall temperatures were observed at low air flow rates. A correlation for the heat-transfer coefficients was obtained. The pressure drop data agreed well with the Lockhart–Martinelli correlation and the prediction of the Wrobel–McManus wave roughness theory.

NOMENCLATURE

A, tube cross-sectional area [ft^2];
D, tube diameter [ft];
g_0, proportionality constant in Newton's law [lbft/lbfs^2];
h, local heat-transfer coefficient [Btu/hft^2 °F];
$\bar{h}$, average heat-transfer coefficient;
k, thermal conductivity [Btu/hft°F];
L, refers to a specific axial distance [ft], used in $\Delta P/L$, etc.;
Nu, Nusselt number;
P, pressure [lbf/ft^2];
$\Delta P/L$, pressure drop per unit length [lbf/ft^3];
$\Delta P_m/L$, momentum pressure drop per unit length;
Pr, Prandtl number;
q, heat-transfer rate [Btu/h];
$\dot{q}$, heat flux [Btu/hft^2];
r, refers to radial distance from tube axis [ft];
Re, Reynolds number;
T, temperature [°F];
$\bar{u}$, bulk axial velocity [ft/s];
W, specific humidity [lb water vapor/lb air];
$\dot{W}$, flow rate [lb/s];
X, Lockhart–Martinelli two-phase parameter. Square root of the ratio of pressure drop for liquid flowing alone to gas flowing alone in a tube of specified diameter for the specified phase flow rates.

Greek symbols

ρ, density [lb/ft^3];
ϕ_g, ϕ_l, Lockhart–Martinelli parameters equal to the square root of the ratio of two-phase pressure drop to single-phase (phase specified by subscript) pressure drop for the same tube diameter.

Subscripts

bi, refers to two-phase equilibrium state prior to heat addition;
F, refers to final state for thermal and phase equilibrium;
g, refers to gas phase;

* Presently Assistant Professor, Department of Mechanical Engineering, Iowa State University, Ames, Iowa, U.S.A.
† Professor, Sibley School of Mechanical Engineering, Cornell University, Ithaca, New York, U.S.A.

i, refers to inside surface;
l, refers to liquid phase;
t.c., refers to thermocouple location or measurement;
0, refers to wall value;
1, 2, refers to upstream and downstream station, respectively.

Superscript

$\bar{}$ denotes space averaged quantities.

INTRODUCTION

TWO-PHASE flows have been of continuing interest in engineering situations, and with time the need for more accurate data and greater understanding of the phenomena has increased. The engineering endeavors wherein two-phase flows are of interest range from liquid fuel rocket systems to petroleum pipe lines. In this wide spectrum of application, it is to be expected that the parameters of interest will differ widely. This has led to a great diversity in the literature, making comparisons between works tedious, and meaningful generalizations difficult.

Categorizations of two-phase flows have been on the basis of the two phases being chemically similar or dissimilar; i.e. single component, two-component. Further subdivision has been suggested on the basis of the flow regimes of the phases; i.e. laminar or turbulent, with four possible combinations. The flows have also been classified according to flow pattern such as mist, bubble, etc. The flow patterns have been discussed recently by Silvestri [1].

Reasonable correlations of pressure drop have been obtained with parameters that make no important distinction between single component and multicomponent flow [2]. No comparable correlations exist for heat-transfer coefficients. This is not surprising when the complications; e.g. composition effects, pressure effects on saturation, etc., of heat transfer in two-phase systems are considered.

Reports of experimental works with horizontal two-component, two-phase flows with heat transfer are extremely limited when the wide range of flow parameters possible and engineering interest is considered. Johnson and Abou-Sabe [3], King [4], and Fried [5] have all investigated heat transfer in air–water mixtures in heated horizontal tubes. The bulk of these data are for slug or sluggish–annular flows. Johnson [6] has also worked with air–oil flows.

Results from investigations of one-component flows tend to suggest possible two-component behavior but, as yet, no correlation or theory has been sufficiently general to treat heat transfer in both types of flow. Much of the recent one-component data in the pure convection regime appears to be well correlated by an expression presented by Davis and David [7]. The Davis and David expression does not even come close to correlating the present horizontal two-component data even though it has been reported [7] to result in predicted heat-transfer coefficients which agree reasonably well with the vertical flow results for the air–water system studied by Groothuis and Hendal [8]. Although the possible flow patterns of one and two-component flows are similar, the heat-transfer mechanisms in the liquid film may be basically different since the one-component system is always at or near the saturation temperature and evaporation is much more frequently accompanied by the physical agitation which is characteristic of boiling.

This paper is primarily concerned with an experimental investigation of heat transfer to horizontal annular two-phase, two-component flow. The experimental apparatus used in the present investigation differed substantially from any used in previous heat-transfer studies in this type of flow, and the majority of data taken was in a flow regime for which no previous heat-transfer study had been reported.

GENERAL APPARATUS AND INSTRUMENTATION

A schematic diagram of the experimental apparatus is given in Fig. 1. Details of the apparatus are given in [9].

The straight run of pipe following the orifice was of sufficient length to give a fully developed velocity profile at the mixing section. The mixing device, Fig. 2, introduced the liquid as an annulus of 0·015 in thickness at point of contact with the air stream. The test section consisted of 105·625 in of clear acrylic tubing with a nominal I.D. of 1 in followed by a heating section of stainless steel with an O.D. of 2 in. The heating section was located in a region known to be free of entrance effects. The test section was completed with a 53-in length of acrylic leading to a liquid–gas separator. End losses in the heat-transfer section were minimized by using insulating material for flanges.

Pressure taps, situated in the bottom of the test section, were located at eight stations. Pressures were measured with gauges and mercury-under-water manometers. A recirculating system was used for the liquid and liquid flow rates were set with rotameters and measured by weigh tanks.

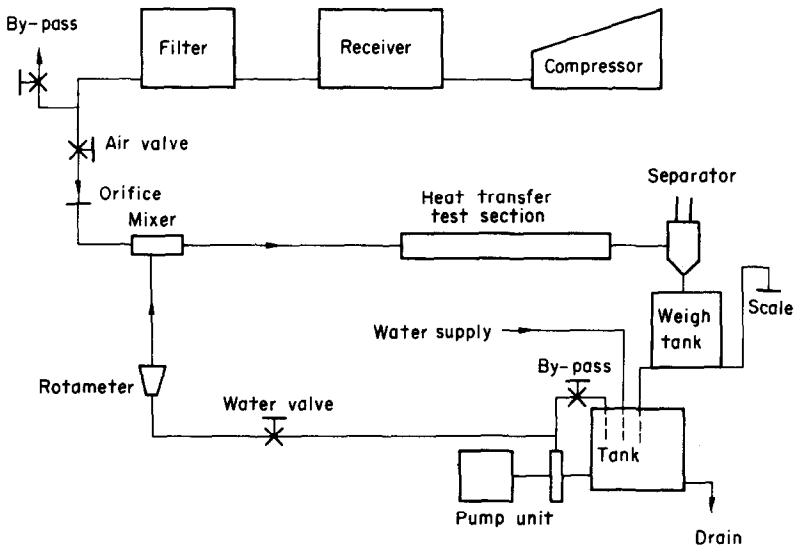

FIG. 1. Schematic diagram of experimental arrangement.

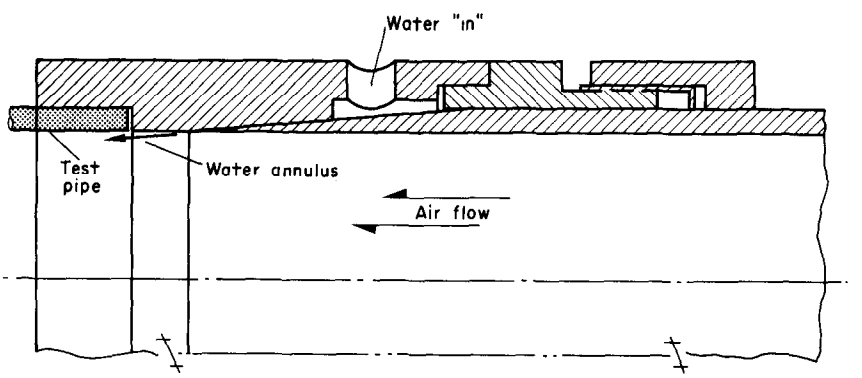

FIG. 2. Detail of mixing device.

Heat-transfer section

Stainless steel was chosen for the test section because of its relatively low thermal conductivity compared to other metals so that any circumferential variation in heat-transfer coefficient would be more easily detected through a circumferential tube wall temperature distribution. A thick wall tube was used so that the temperature differences across the tube wall would be measurable, allowing a calculation of local heat flows.

Temperature measuring stations were located at 6-in intervals along the tube with extra stations positioned 1 in and 3 in from each end providing temperature information for a total of thirteen axial locations. The test section

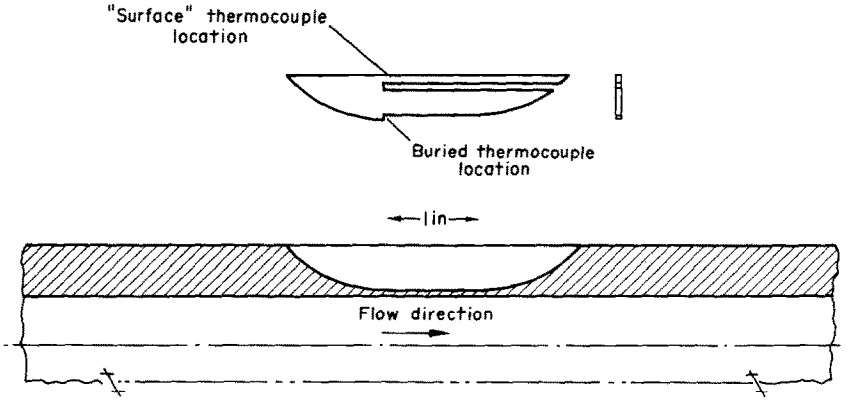

FIG. 3. Test section slot and plug detail.

thermocouples were made from 30-gauge chromel–alumel wire. The buried thermocouples were located at the bottom of longitudinal slots milled in the stainless tube. The slots were 0·045 in wide, 0·450 in deep and, except for the two stations nearest each end which were spaced more closely together, about 3 in long at the surface. The buried thermocouples were cemented to the bottom of stainless steel plugs designed to fit snugly into the slots. Figure 3 illustrates this arrangement. This slot and plug method of installing thermocouples was used instead of some simpler method, such as drilling radial holes, because the axial temperature gradient was small compared to the radial or even circumferential gradient.

The buried thermocouples, installed as described above, provided the primary temperature data for the test section. No true surface thermocouples were installed, but rather several thermocouples were cemented in longitudinal slots milled in the plugs so that the thermocouple junctions would be near the surface, 0·1 in. Where both thermocouples were installed in the same plug, it was possible to determine temperatures at two radial locations 0·335 in apart which enabled the temperature gradient to be computed. The junctions were electrically insulated so that the thermocouples could be connected to indicate a differential temperature. All thermocouples were cemented in place with Technical "G" Copper Cement. This cement is a good electrical insulator while being a fair thermal conductor.

The slots were located at several circumferential positions at each axial station in order to determine the circumferential temperature distribution. The temperature distribution is not expected to be symmetric for horizontal annular two-phase flow due to the gravity-caused eccentricity of the liquid film. The flow and tube wall temperature distribution should, however, be

symmetric about the vertical plane containing the tube axis. Thus the majority of the thermocouples were located on one side of the tube with only a few on the opposite side to check the symmetry. The design called for fifty-eight buried and twenty-three surface thermocouples. The location of thermocouples is given in Fig. 4.

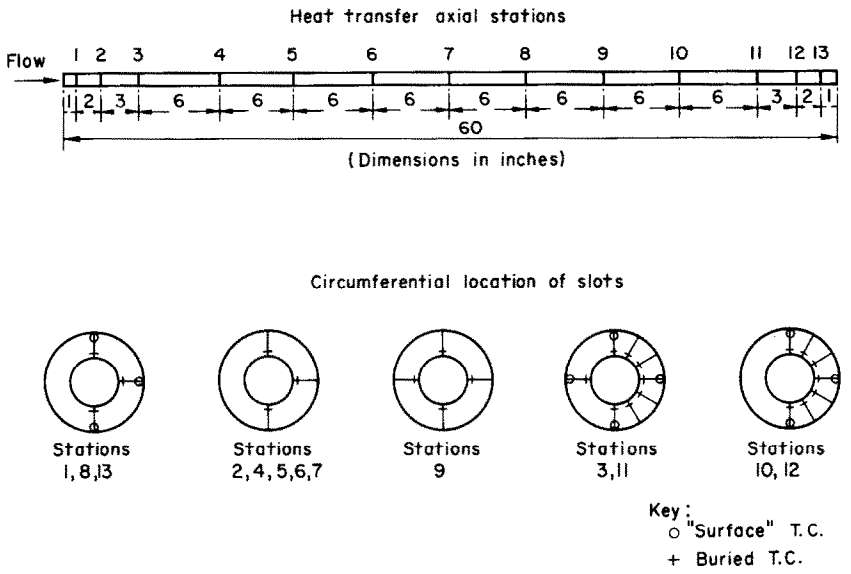

FIG. 4. Location of thermocouples in test section (dimensions in inches).

Fiberglass insulated Nichrome V wire was used to heat the tube. Both molded and blanket fiberglass insulation were applied over the heating wires to minimize heat loss from the installation. Direct current was used for heating. Voltage and current measurements were used to compute power input.

Temperatures other than those in the test section proper were measured with copper–constantan thermocouples and/or conventional thermometers. Wet bulb determinations were made at air exhaust and inlet for evaluation of humidity.

EXPERIMENTAL PROCEDURES

Several single-phase heat-transfer runs were made with air only to check the characteristics of the apparatus. Air runs were made both before and after the two-phase runs. Heat balances for all but one run were within ± 10 per cent and the measured coefficients for air agreed to within ± 10 per cent of the predictions of the modified Sieder–Tate correlation [10]. With only a few isolated exceptions, symmetry about the tube axis prevailed in the temperatures indicated by the circumferentially spaced thermocouples. The results from the air runs are presented and discussed in [9].

Forty-nine water–air two-phase heat-transfer runs were made. The water flow rate varied from 0·0714 to 0·3836 lb/s and the gas flow rate from 0·0300 to 0·2573 lb/s. This range in gas flow rate corresponded to an approximate gas Reynolds number range of from 36000 to 320000. All gas Reynolds numbers were computed using the full tube diameter of 1 in. The heat flux varied from 7372 to 12772 Btu/hft^2. An energy balance was made for each run which took into account the evaporation process since for some runs more than half of the heat added to the mixture in the test section was accounted

for by the latent heat of vaporization. Heat-transfer coefficients were repeatable to within 4 per cent. Additional details concerning the experimental procedure as well as specific operating conditions for each run are given in [9].

PRESENTATION AND DISCUSSION OF RESULTS

Pressure drop

Although the pressure drop measurements were not the prime objective of the investigation, they are of considerable interest since existing correlations and theories still do not allow predictions to within the desired engineering tolerances. The readings were corrected for momentum effects so as to yield, as closely as possible, the friction pressure drop. Although readings from all eight pressure taps were recorded, the pressure drop of main interest and the one presented here was the one which spanned the heat-transfer test section. For the heat fluxes used, pressure drop readings changed only slightly from the isothermal measurements. The change was attributable to momentum effects. Corrections for momentum pressure drop in two-phase flows are somewhat arbitrary in that the velocity and phase distributions are not usually known in sufficient detail to compute with certainty the momentum change in the flow from cross-section to cross-section.

In computing the momentum pressure drop, it was assumed that the liquid distribution did not change appreciably over the pressure drop length, as is reasonable for well-developed annular flow. From this it follows that the average liquid velocity does not change over this length and that the momentum pressure drop is due to velocity changes in the gas phase. In computing the gas average velocities, the area occupied by the liquid annulus was neglected. Using subscripts 1 and 2 for the upstream and downstream stations, respectively,

$$\Delta P_m = \rho_2 \bar{u}_2^2 - \rho_1 \bar{u}_1^2 \tag{1}$$

where, as is customary, the average gas velocity squared is used rather than the average over the cross-section of the local velocity squared.

It is assumed that the air–water mixture comes very close to attaining a uniform temperature with the air saturated with water vapor at the entrance to the heat-transfer section. Experimental verification of this process was obtained by making adiabatic two-phase runs and comparing the inlet tube wall temperature to the computed fluid temperature at that point. Properties at the downstream pressure drop station were evaluated at the experimentally determined mixing cup temperature.

Using the continuity equation and the ideal gas law, the momentum pressure drop can be determined from

$$\Delta P_m = \frac{\dot{W}_a^2}{g_0 A^2}\left[\frac{(1 + W_2)^2}{\rho_2} - \frac{(1 + W_1)^2}{\rho_1}\right] \tag{2}$$

or, since $\rho = \rho_a(1 + W)$,

$$\Delta P_m = \frac{\dot{W}_a^2}{g_0 A^2}\left[\frac{1 + W_2}{\rho_{a2}} - \frac{1 + W_1}{\rho_{a1}}\right] \tag{3}$$

where $\dot{W}_a$ is the flow rate of dry air and W is the specific humidity.

Comparison with existing correlations

Flow conditions and the main pressure drop parameters are tabulated in [9]. Figure 5 shows the pressure drop data plotted on Lockhart–Martinelli [11] coordinates. The solid line is that given by Lockhart and Martinelli for turbulent–turbulent flow. The parameters X, ϕ_l, and ϕ_g have been corrected for momentum effects.

The results of the Wrobel–McManus [12] wave roughness theory as applied to the experimental flow conditions are shown also in Fig. 5. It is quite noteworthy that the results of this theory fall so close to the Lockhart–Martinelli correlation line. A comparison of this sort has not been observed in the literature before.

Figure 6 shows the experimental data plotted according to the modification to the Lockhart–Martinelli correlation proposed by McMillan,

Fontaine and Chaddock [2]. Only those experimental points which were within the reported range of validity of this modification were plotted. The modification maintains the form of the Lockhart–Martinelli correlation but suggests that the method of computation of gas pressure drop in the denominator of ϕ_g be modified to take into account the effect of surface roughness due to the presence of waves.

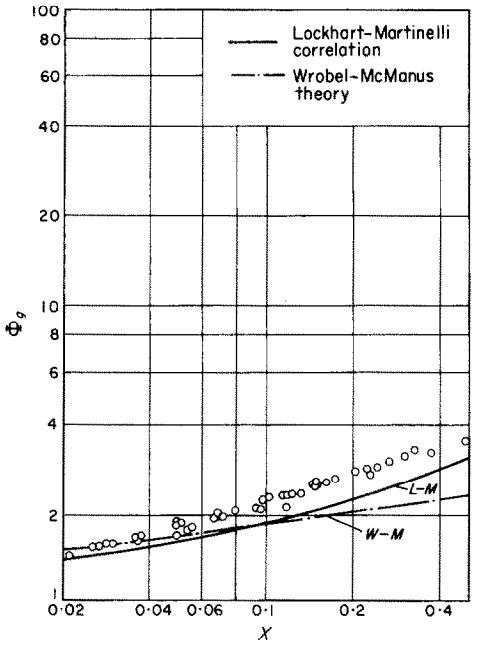

FIG. 5. Pressure drop data on $\phi_g - X$ coordinates; comparisons with theories and correlations.

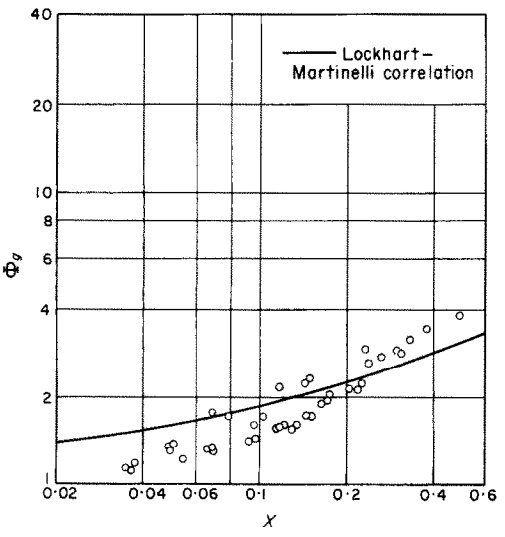

FIG. 6. Modification proposed in [2] applied to pressure drop data on $\phi_g - X$ coordinates.

The modified ϕ_g should then, according to the intent of [2], put the data in better agreement with the Lockhart–Martinelli line. It appears the modification overcorrected for low values of X and generally gave rise to a greater vertical spread in the points than in the unmodified plot of Fig. 5. It should be pointed out that deviations in plots on ϕ_g–X coordinates can be misleading in the sense that a given percentage change in two-phase pressure drop for fixed-flow conditions will result in only about half that percentage change in ϕ_g since ϕ_g depends upon the square root of the two-phase pressure drop.

Two-phase heat-transfer experimental results

Local and the overall or average heat-transfer coefficients were evaluated experimentally. The local heat-transfer coefficient is defined according to

$$h = \dot{q}/(T_0 - T_F), \tag{4}$$

where T_F is the equilibrium temperature for phase as well as thermal equilibrium. In the present experiments, T_F for $L/D = 60$ was measured in the cyclone separator where the two phases were well mixed. At all other axial stations, T_F was computed from the inlet conditions and measured heat input of the test section. The T_0 used in the computation of local coefficients was determined from solving the conduction problem through the tube wall assuming uniform heat flux resulting in

$$T_0 = T_{\text{t.c.}} - \frac{q \ln (r_{\text{t.c.}}/r_i)}{2\pi k L} \tag{5}$$

where $T_{\text{t.c.}}$ is the average of the buried thermocouple readings at the axial location of interest except for $L/D = 60$, where the linear portion of axial temperature distribution was extrapolated to the end of the tube to compensate

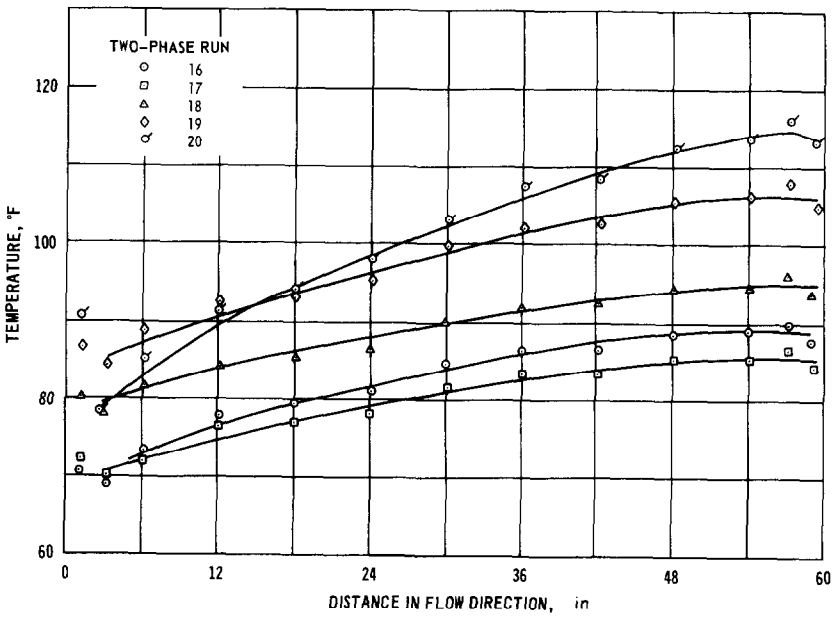

FIG. 7. Representative axial wall temperature distributions for two-phase heat-transfer runs.

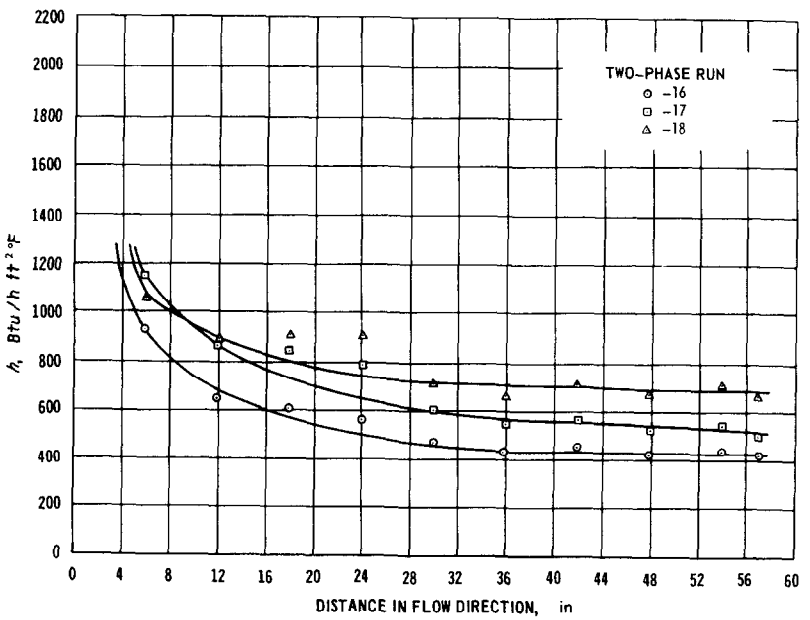

FIG. 8. Representative axial distributions of local heat-transfer coefficient for two-phase heat-transfer runs.

for end effects. Here, q is the heat flow in Btu/h, $r_{t.c.}$ and r_i are the radial distances of the thermocouple location and the inside tube surface from the tube axis, respectively, L the tube length and k the thermal conductivity of the stainless tube. The metal thermal conductivity was evaluated by the experimentally determined relationship presented by Allen and Eckert [13].

The average coefficient is defined by

$$\bar{h} = \dot{q}/(\bar{T}_0 - \bar{T}_F), \tag{6}$$

where $\bar{T}_0$ is the integrated average inside surface or wall temperature, and $\bar{T}_F$ is the average of the inlet equilibrium temperature and the final measured equilibrium temperature.

Typical axial temperature distributions are shown in Fig. 7. The temperature profiles are somewhat flatter than would be expected without taking into account the evaporation process. Typical axial distributions of the local heat-transfer coefficient are shown in Fig. 8. It is interesting to note that the local heat-transfer coefficients do tend toward a value independent of length which suggests a tendency for the annular two-phase flows to attain a type of fully developed condition. This approach to a constant coefficient also tends to substantiate the physical significance of the equilibrium temperature defined above. The major portion of the discussion concerning local coefficients will be confined to the local coefficient at $L/D = 60$.

Figure 9 shows the experimental local heat-transfer coefficient at $L/D = 60$ plotted against gas Reynolds number for various nominal water flow rates. The dashed lines at the left of the figure show the expected behavior of the coefficients as the limiting condition of no gas flow is approached. The limit at zero gas flow was computed for the particular water rate flowing alone in the tube.

The method of plotting in Fig. 9 illustrates several interesting characteristics of the heat-transfer coefficients. The two-phase coefficients were always greater than the corresponding single-phase coefficients. It appears that, for a given water rate, the coefficient can be increased several times by forming a two-phase flow with air. The coefficients reach a maximum at a

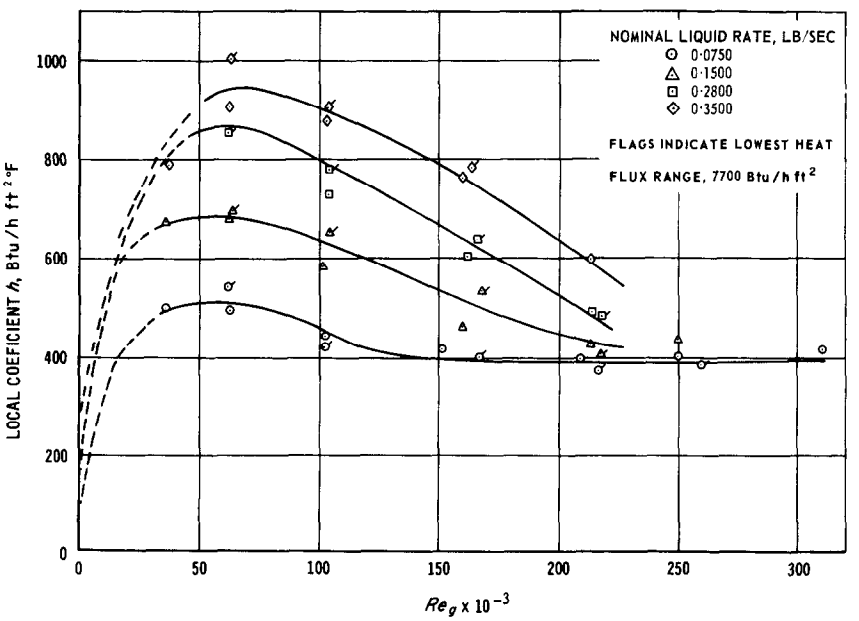

FIG. 9. Local heat-transfer coefficients for the two-phase runs at $L/D = 60$.

relatively low air flow rate and drop off sharply with increasing air rate. Johnson and Abou-Sabe [3] also observed a tendency for maxima in a similar plot of their data but their peaks were less sharply defined than those in Fig. 9. Maxima in heat-transfer coefficients have also occurred in vertical two-component flow [8]. Part of the scatter in Fig. 9 is caused by the variations of the actual water flow rates from the nominal values, The coefficients are quite sensitive to small changes in water rates, especially at the lower air flow rates.

The trends in the coefficients observable in Fig. 9 can be explained qualitatively as follows. As air is added to a flow of water, the transfer mechanisms are intensified considerably, as evidenced by the fact that the two-phase pressure drops may be as much as 100 times the pressure drops for water flowing alone in the tube. The intensified transport mechanisms result in much higher heat-transfer coefficients. As the air flow rate continues to increase for a fixed water flow rate, the flow pattern changes, as well as the transport mechanisms so that a given increase in air rate will cause less of an increase in pressure drop and the heat-transfer coefficient than previously. This is confirmed for pressure drop by experimental evidence. Also as the air rate increases a countering mechanism comes into play which tends to reduce the heat-transfer coefficient by depressing the final equilibrium temperature, T_F. This occurs since, as the ratio of air flow rate to water flow rate increases, more and more evaporation is possible. At some air flow rate, this latter mechanism begins to dominate. The coefficient passes through a maximum for the given water rate and then decreases as the air rate increases. Liquid entrainment at the higher air rates also tends to depress the coefficient.

Groothuis and Hendal [8], who could not observe the flow pattern in their apparatus, suggested that the maximum in the heat-transfer coefficient might coincide with the flow condition at which randomly distributed dry spots appeared at the walls. They suggested that this maximum might occur for a constant value of the Weber number. Visual observations were made in the present experiments and dry spots were not found to occur coincident with the maximum in heat-transfer coefficient. It is believed that liquid entrainment, for which the Weber number is also expected to be an important parameter, as well as the other effects mentioned in the previous paragraph, are more likely to cause the maximum in heat-transfer coefficient than are the occurrence of dry spots.

Observation of circumferential variations

For low air rates where the liquid film is known to be most eccentric [14], sizable circumferential temperature variations were observed in the tube wall. The measurements always showed the coldest part of the tube circumference to be at the bottom. In turn, this indicates that the local coefficient is greatest at the bottom since the temperature difference between the wall and the bulk fluid would be smallest there. These temperature variations for axial station 11 rounded off to the nearest degree are tabulated in [9] for each two-phase heat-transfer run. Axial symmetry in the experimental setup was well verified from the results of the single-phase air runs, as was discussed in a previous section. Thus the tube wall temperature variations were caused by variations in the local coefficient around the tube. The variations in temperature characteristically persisted at about the same order of magnitude at all the axial measuring stations so that it was not a phenomenon associated only with the entrance length or developed flow length of the heat-transfer section.

It is of interest to note that in horizontal one-component flow, the circumferential variation in the local heat-transfer coefficient is apparently generally the opposite of the two-component variation as can be seen from the results shown in [15]. This seems reasonable since the major thermal resistance occurs at the gas–liquid interface in the annular air–water

system. Thus, the wavier surface at the bottom (due to gravity caused film eccentricity) promotes an intensified heat-transfer mechanism and a reduced interfacial resistance. In annular one-component flow, the major thermal resistance is through the liquid film which is smaller at the top causing a maximum in the heat-transfer coefficient at that location.

Although the circumferential variations in tube wall temperature and local coefficients are related to film eccentricity, the exact mechanisms by which the film eccentricity produces variations in the local coefficients are not known. Two effects which are thought to be important in this regard are discussed in [9].

The circumferential variation in the local heat-transfer coefficient cannot be determined directly from the measured temperatures based on the buried thermocouple readings since the variations in inside wall temperature will also cause the heat flux to be asymmetrical about the tube axis. To obtain a qualitative picture of the circumferential variations in local heat flux associated with a measured circumferential temperature variation, the conduction problem in the tube wall was solved numerically. It was assumed that symmetry existed about the vertical plane through the tube axis. Rather

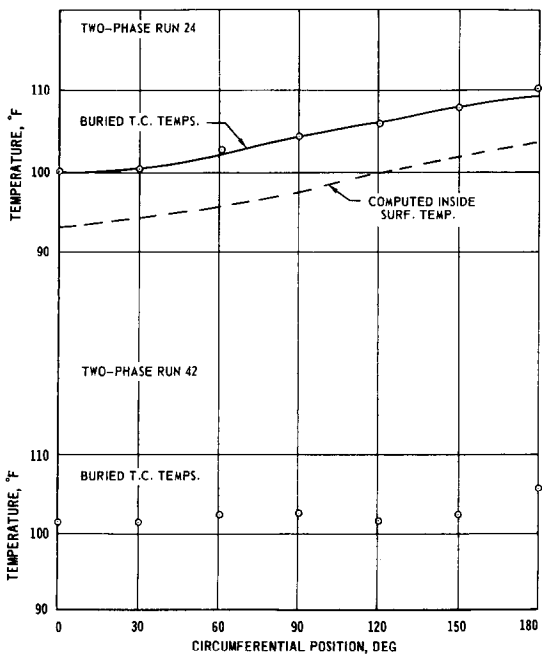

FIG. 10. Measured and computed circumferential temperature distributions, axial station 11, two-phase runs 24, 42.

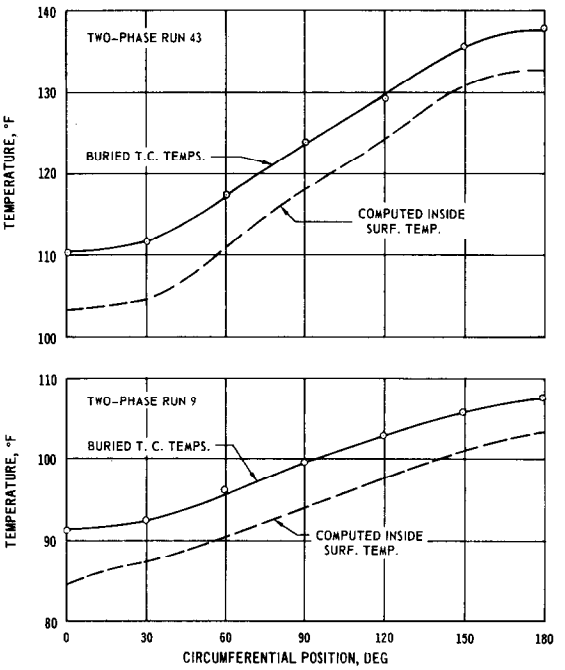

FIG. 11. Measured and computed circumferential temperature distributions, axial station 11, two-phase runs 9, 43.

standard finite difference methods were used in the numerical solution. The methods are described in more detail in [9]. The computations were done by using an iterative procedure on the digital computer.

Figures 10 and 11 show the measured circumferential temperature distribution at axial station 11 for two-phase runs 9, 24, 42 and 43. The conduction problem was solved numerically for runs 9, 24 and 43 so that the smooth curves drawn through the points are the same curves used to determine the input for the numerical solution mentioned above. The dashed curves in Figs. 10 and 11 represent the inside surface

temperatures obtained from the numerical solution of the conduction problem. The temperature variations from runs 9, 24 and 43 are representative samples covering the range of circumferential temperature variations observed.

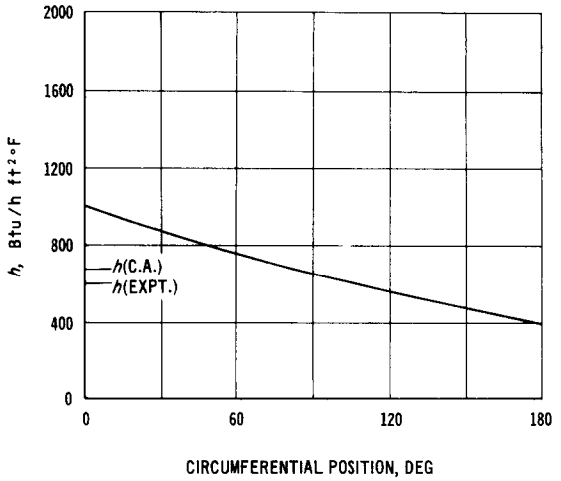

FIG. 12. Computed circumferential distribution of local heat-transfer coefficient, axial station 11, two-phase run 24.

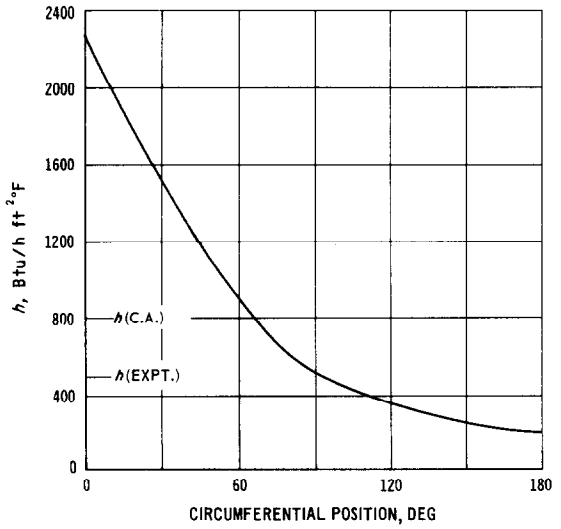

FIG. 13. Computed circumferential distribution of local heat-transfer coefficient, axial station 11, two-phase run 43.

Figures 12 and 13 show the circumferential variations in the local coefficient computed from the results of the numerical conduction solution for runs 24 and 43. The integrated average coefficient, determined by numerically integrating the computed circumferential coefficient distribution, is noted for each run as well as the experimentally determined coefficient computed on the basis of equation (4) which used the arithmetic average buried thermocouple temperature extrapolated to the inside surface by use of the conduction equation. This equation allows for the assumption that the heat flux is uniform around the circumference. The former average coefficient is seen to be somewhat higher than the latter. A comparison

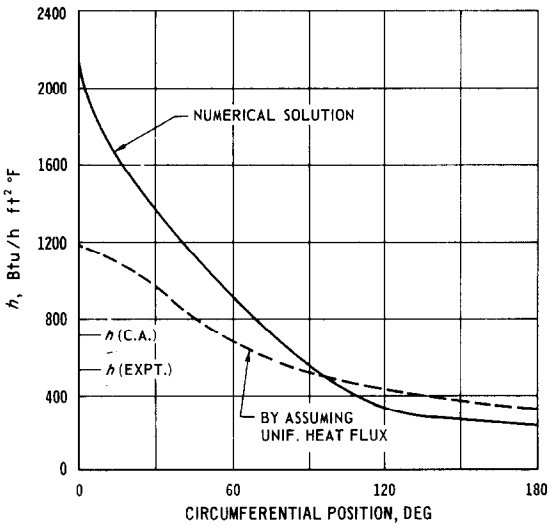

FIG. 14. Computed circumferential distribution of local heat-transfer coefficient, axial station 11, two-phase run 9.

of the circumferential distribution of h from the numerical solution and that which results from extrapolating each measured temperature to the wall based on an assumed uniform heat flux is given in Fig. 14. This illustrates the effect of the circumferential variation in heat flux on the circumferential distribution of the local heat-transfer coefficient.

Circumferential variations in tube temperatures and heat fluxes are important in applications and some interest in these matters has been observed recently in the literature [16]. A

noteworthy aspect of the circumferential variation in heat-transfer coefficient is that the resulting circumferential variation in tube temperature will depend heavily on the thermal conductivity of the tube material. The greater the thermal conductivity, the smaller the observed temperature variation.

Generalization of data

Johnson and Abou-Sabe [3] were able to correlate most of their data to within ± 20 per cent by plotting $\bar{h}/\bar{h}_l\phi_l^2$ against X where $\bar{h}$ is based on the logarithmic mean temperature difference (LMTD). The average coefficient, $\bar{h}$, for the present work has been previously defined and is not based on the LMTD since there is little physical justification for the use of the LMTD in the heat-transfer system under study.

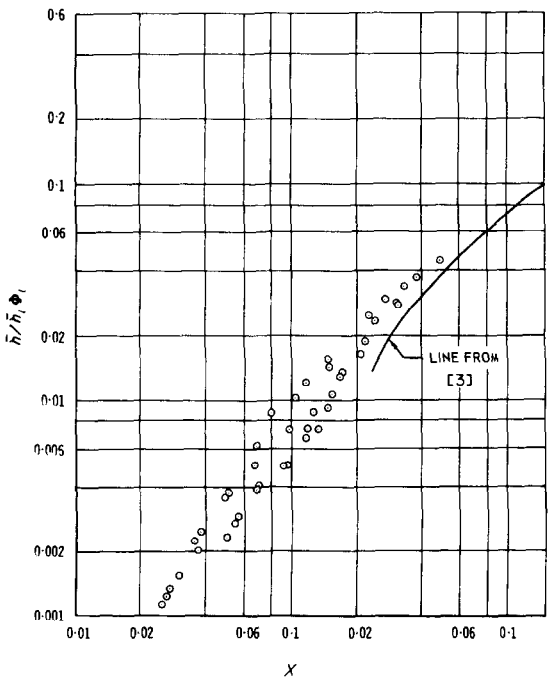

FIG. 15. Comparison of present heat-transfer data with the correlation suggested by Johnson and Abou-Sabe.

Figure 15 shows the present data plotted according to $\bar{h}/\bar{h}_l\phi_l^2 - X$ coordinates suggested in [3] except that the $\bar{h}$ is not based on the LMTD. The solid line shown in Fig. 15 is the line given by Johnson and Abou-Sabe [3] representing an average of their data. The coefficient $\bar{h}_l$ was computed from $Nu = 0{\cdot}023\ Re^{0{\cdot}8}Pr^{0{\cdot}4}$ where Re was computed on the basis of the specified flow rate and the tube diameter. On the basis of the X coordinate, there is very little overlap between the present data and that of Johnson and Abou-Sabe [3], but the coordinates suggested by them do a reasonably good job of correlating the data. In the limited region of overlap, the present data all fall above the line, [3].

Fried [5] was able to correlate his data as well as that of Johnson and Abou-Sabe [3] by using $\bar{h}/\bar{h}_l - \phi_l^2$ coordinates. He computed a coefficient based on the integrated mean temperature difference as well as the LMTD and found that the coefficients based on the former temperature difference were always lower. Figure 16 shows the present data plotted according to the $h/h_l - \phi_l^2$ coordinates. The solid line represents the average given by Fried for his data for the range of the abscissa used in Fig. 16. The present experimental points tend to group about the Fried line but the scatter is so great that the parameters cannot be considered as providing a good correlation for the present data.

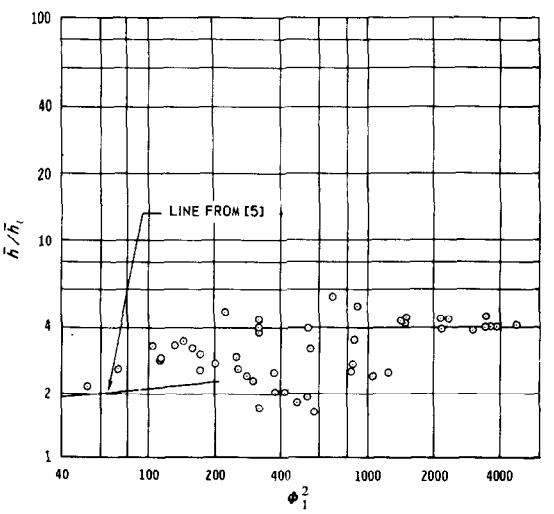

FIG. 16. Comparison of the present data with the correlation suggested by Fried.

Several arbitrary parameters were tried in an attempt to obtain the best correlation of the present data. Due to the complexity of the system, it has been impossible to arrive at a simple grouping of the important parameters through the usual procedures using dimensional analysis. Since the heat-transfer coefficient is nearly always related to friction in convective systems, it is expected that the two-phase heat-transfer coefficient should depend upon the relative flow rates and physical properties of the two phases. Thus the pressure drop parameters such as ϕ_l, ϕ_g, and X can be expected to have some relevance for heat-transfer correlations. The way in which the Reynolds analogy must be modified for annular two-phase flows is thought to be similar to that for heat transfer to rough surfaces and is discussed in [9].

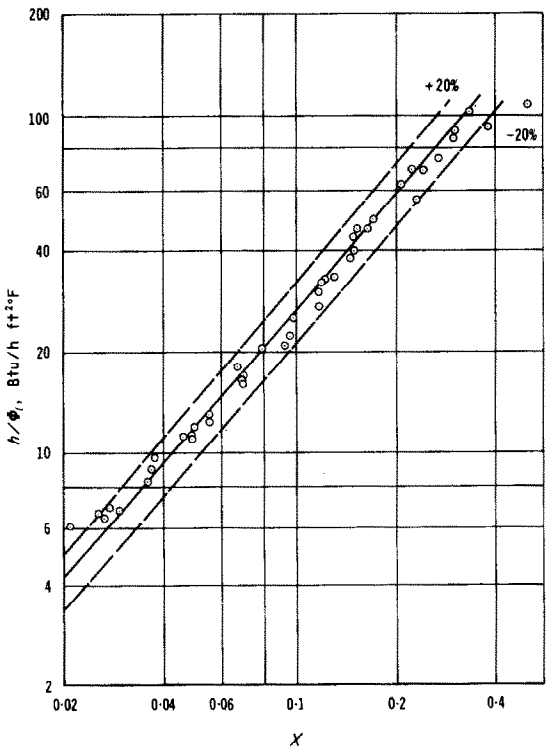

FIG. 17. Correlation of measured local heat-transfer coefficient based on X.

Two reasonably good correlations were found for both the local and the average coefficient. Figure 17 shows the local coefficients from the present investigation correlated by plotting h/ϕ_l against the Lockhart–Martinelli X. Figure 18 shows a similar plot, but for the average

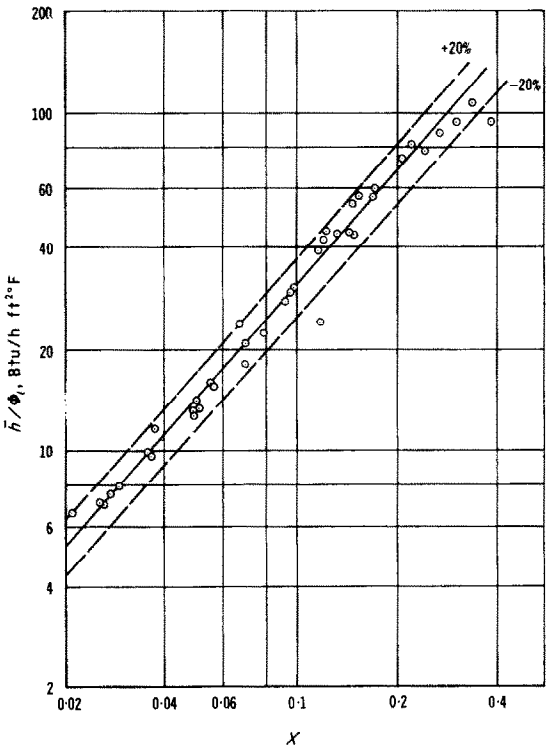

FIG. 18. Correlation of measured average heat-transfer coefficient based on X.

coefficient, $\bar{h}$. In both correlations, almost all of the points fall within ± 20 per cent of the best straight line through the data. A slightly better correlation was obtained by plotting h/ϕ_l and $\bar{h}/\phi_l$ against $X(\dot{W}a/W_l)^{0.4}$. These latter plots can be seen in Figs. 19 and 20.

Figure 21 shows some of the results from [3,5] plotted according to the $\bar{h}/\phi_l - X$ coordinates which provided a good correlation for the present data. The solid line is the same as shown in Fig. 18, and the cross-hatched band represents the region in which the present

data fell. Fried's data [5] were presented in such a way that the parameters for Fig. 21 could be computed directly without making any additional assumptions. The values of $\bar{h}$ based on the integrated mean temperature difference were used. The values of $\bar{h}$ and X had to be computed from the basic flow rates,

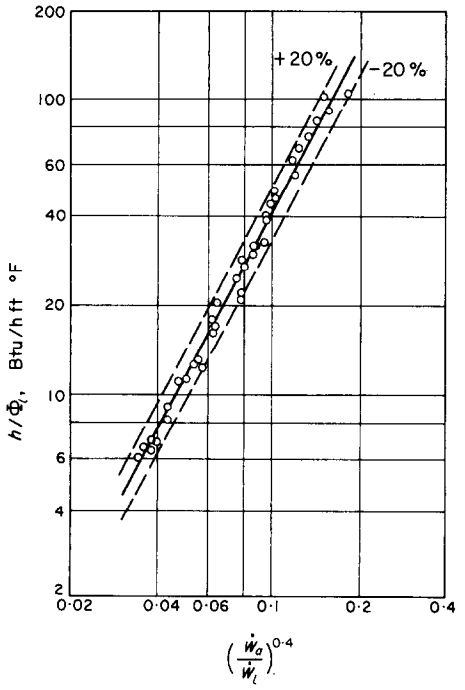

FIG. 19. Correlation of measured local heat-transfer coefficient based on $X(\dot{W}_a/\dot{W}_l)^{0.4}$

temperatures, and heat fluxes in the case of the Johnson and Abou-Sabe data. In doing this it was assumed that the air was saturated with water vapor at the inlet and exit of the heat-transfer section and that the reported wall temperature was the integrated average temperature. With these assumptions, the average coefficient could be computed according to equation (7). Only the data from [3, 5] which came the closest to the annular regime are included in Fig. 21. The data of these other investigators are not well correlated by these coordinates, although the data does group near the solid line.

The general agreement of the present data with that of other investigators is believed to be good considering that the data are largely from two different flow regimes, the annular regime in the case of the present investigations and the slug flow or sluggish–annular regimes for [3, 5]. Also there was some uncertainty in arriving at an appropriate temperature difference to use in computing the coefficients for the comparisons.

The parameter h/ϕ_l used to correlate the experimental data is not dimensionless. In single-phase pipe flows, the heat-transfer coefficient is most often generalized through the use of the Nusselt number, $Nu = hD/k$, which

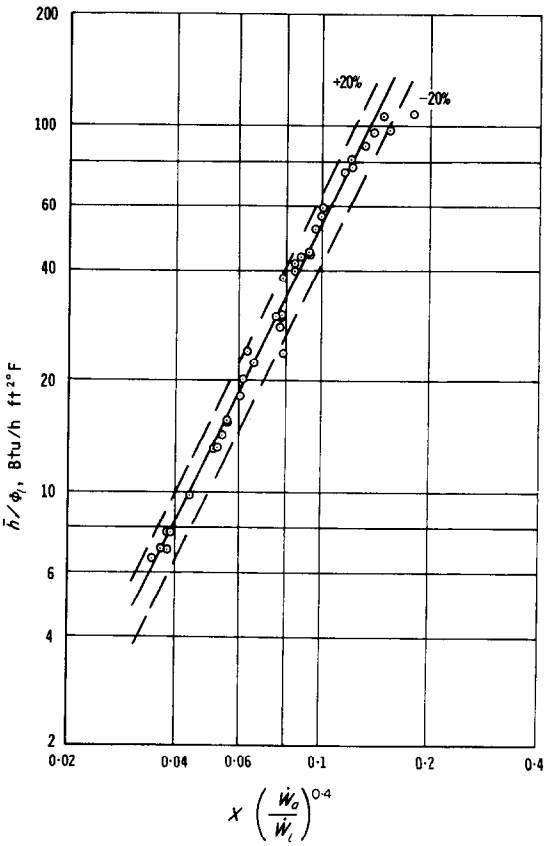

FIG. 20. Correlation of measured average heat-transfer coefficient based on $X(\dot{W}_a/\dot{W}_l)^{0.4}$.

is characteristically a function of the Reynolds and Prandtl numbers. The effects of mass transfer prevent this type of generalization from being exact for the present conditions, so that the use of the Nusselt number would have been misleading. This point is discussed in some

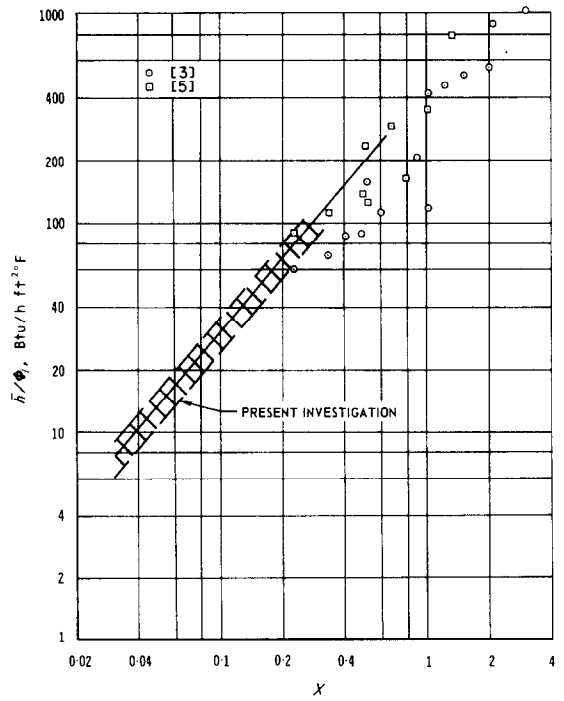

FIG. 21. Comparison of data of other investigators with $\bar{h}/\phi_l - X$ correlation.

detail in [9]. The most important two-phase heat-transfer parameters from the experimental program are also tabulated in detail in [9].

SUMMARY OF RESULTS AND CONCLUSIONS

1. The pressure drop measurements for the heat-transfer runs agreed well with those of other investigators, both isothermal and with heat transfer, as indicated by the same relative agreement with the Lockhart–Martinelli correlation as generally obtained by others. The Wrobel–McManus wave roughness theory produced predictions which agreed surprisingly well with the Lockhart–Martinelli correlation. For the range of the present experiments, the Wrobel–McManus theory allowed predictions of pressure drop which agreed better with experiment than predictions based on the Lockhart–Martinelli correlation for $X < 0{\cdot}1$, which corresponds to the range in which the model upon which the theory was based most nearly agrees with the experimentally observed conditions. An application of the modification to the Lockhart–Martinelli correlation proposed by McMillan, Fontaine and Chaddock [2] resulted in the data group being more nearly centred about the correlation line, but the general scatter in the data was increased.

2. The investigation covered a range of two-phase, two-component flows over most of which no previous heat-transfer studies are known to exist. Where the present work came closest to overlapping the range investigated by others, the agreement between the present work and that of other investigators was reasonably good considering the differences in the experimental setups and procedures. The two-phase local coefficients ranged from about 400 to 1000 Btu/h ft^2 and were in all cases greater than the computed coefficients for either phase flowing alone in the tube. The local heat-transfer coefficients were correlated very well by plots on $h/\phi_l - X$ and $h/\phi_l - X(\dot{W}_a/\dot{W}_l)^{0{\cdot}4}$ coordinates. The average coefficients were correlated well also with the above coordinates when h was replaced by $\bar{h}$. All but a very few points fell within ± 20 per cent of the best line through the data plotted as indicated above. The use of $X(\dot{W}_a/\dot{W}_l)^{0{\cdot}4}$ provided the better correlation of the two. As the air rate was increased from zero for a fixed water rate, the heat-transfer coefficient increased and passed through a maximum. The coefficient then decreased with increasing air rate, the more so for the higher water rates, so that the coefficients for the various water rates tended to converge for the higher air rates. The local coefficients

were observed to approach a value independent of axial distance.

3. At low air rates and generally for flow conditions near the maximum in the coefficient mentioned above, significant circumferential temperature variations were measured in the tube. These were as great as 26 degF for one run. Due to the inherent coupling between the circumferential temperature variation and the heat flux, the conduction problem was solved numerically in the tube at one axial station for three representative runs to provide at least a qualitative measure of the distribution of the local coefficient. These results indicated variations in the local coefficients around the circumference up to ten-fold.

ACKNOWLEDGEMENT

This work was supported in part by a grant from the Army Research Office (Durham).

REFERENCES

1. M. SILVESTRI, Fluid mechanics and heat transfer of two-phase annular-dispersed flow, *Adv. Heat Transf.* **1**, 355 (1964).
2. H. K. MCMILLAN, W. E. FONTAINE and J. B. CHADDOCK, Pressure drop in isothermal two-phase flow—a modification of the Lockhart–Martinelli correlation, ASME Paper No. 64—WA/FE-4 (1964).
3. H. A. JOHNSON and A. H. ABOU-SABE, Heat transfer and pressure drop for turbulent flow of air–water mixtures in a horizontal pipe, *Trans. Am. Soc. Mech. Engrs* **74**, 977 (1952).
4. C. D. G. KING, Heat transfer and pressure drop for water–air mixtures in a 0·737 in I.D. horizontal pipe, M.S. Thesis, University of California, Berkeley (1952).
5. L. FRIED, Pressure drop and heat transfer for two-phase two-component flow, *Chem. Engng Prog. Symp. Ser.* **50**, 47 (1954).
6. H. A. JOHNSON, Heat transfer and pressure drop for viscous–turbulent flow of oil–air mixtures in a horizontal pipe, *Trans. Am. Soc. Mech. Engrs* **77**, 1257 (1955).
7. E. J. DAVIS and M. M. DAVID, Two-phase gas–liquid convection heat transfer, *I/EC Fundamentals* **3**, 111 (1964).
8. H. GROOTHUIS and W. P. HENDAL, Heat transfer in two-phase flow, *Chem. Engng Sci.* **11**, 212 (1959).
9. R. H. PLETCHER, An experimental and analytical study of heat transfer and pressure drop in horizontal annular two-phase, two-component flow, Ph.D. Thesis, Cornell University (1966).
10. F. KREITH, *Principles of Heat Transfer*, p. 347. International Textbook, Scranton, Pa. (1961).
11. R. W. LOCKHART and R. D. MARTINELLI, Proposed correlation of data for isothermal two-phase two-component flow in pipes, *Chem. Engng Prog. Symp. Ser.* **45**, 39 (1949).
12. J. R. WROBEL and H. N. MCMANUS, JR., An analytic study of film depth, wave height, and pressure drop in annular two-phase flow, *Dev. Mech.* **1**, 568 (1961).
13. R. W. ALLEN and E. R. G. ECKERT, Friction and heat transfer measurements to turbulent pipe flow of water ($Pr = 7$ and 8) at uniform wall heat flux, *J. Heat Transfer* **86**, 301 (1964).
14. H. N. MCMANUS, JR., An experimental investigation of liquid distribution and surface character in horizontal annular two-phase flow, ARO(D) Project No. 2117-E, IR 3, Sibley School of Mechanical Engineering, Cornell University (1961).
15. J. B. CHADDOCK and J. A. NOERAGER, Evaporation of refrigerant 12 in a horizontal tube with constant wall heat flux, *Trans. Am. Soc. Heat. Refrig. Air-Condit. Engrs* **73**, 90 (1966).
16. W. A. SUTHERLAND and W. M. KAYS, Heat transfer in an annulus with variable circumferential heat flux, *Int. J. Heat Mass Transfer* **7**, 1187 (1964).

Résumé—On mesure la chute de pression statique en même temps que les coefficients de transport de chaleur locaux et moyens pour un écoulement annulaire horizontal d'eau et d'air dans un tube avec un diamètre intérieur de 25,4 mm. La partie où s'effectue le transport de chaleur est en acier inoxydable chauffé électriquement, a 1,52 m de long et se trouve approximativement à 2,67 m en aval de l'injection du liquide. Les températures de la paroi du tube étaient mesurées à l'aide de 57 thermocouples placés en profondeur et 22 à la surface. Le débit d'eau variait entre 32,4 et 174 g/s; le débit d'air entre 13,6 et 117 g/s; et le flux de chaleur entre 23,25 et 40,3 kW/m^2. On a observé pour de faibles débits d'air de grandes variations le long de la circonférence des températures de la paroi du tube. Une corrélation a été obtenue pour les coefficients de transport de chaleur. Les résultats de perte de charge étaient en bon accord avec la corrélation de Lockhart–Martinelli et la prévision de la théorie de rugosité d'onde de Wrobel–McManus.

Zusammenfassung—An einem Rohr mit der lichten Weite von 25 mm wurden der statische Druckabfall, der örtliche und der mittlere Wärmeübergangskoeffizient für die horizontale Ringströmung von Wasser und Luft gemessen. Die elektrisch beheizte Wärmeübergangsstrecke aus rostfreiem Stahl war 1,5 m lang und lag ungefähr 2,6 m stromabwärts vom Flüssigkeitseintritt. Die Rohrwandtemperaturen wurden mit 57 eingelassenen und 22 an der Oberfläche befestigten Thermoelementen gemessen. Der Massenstrom des Wassers variierte von 3,239 bis 173,9 g/s, der Massenstrom der Luft von 1,361 bis 116,7 g/s und der Wärme-

strom von 23,25 bis 40,28 W/m^2. Bei geringen Luftdurchsätzen wurden beachtliche Unterschiede der Rohrwandtemperatur in Umfangsrichtung beobachtet. Für den Wärmeübergangskoeffizienten wurde eine Gleichung aufgestellt. Die Werte für den Druckabfall stimmten gut mit der Gleichung von Lockart–Martinelli und den Berechnungen nach der Wellen-Rauhigkeitstheorie von Wrobel–McManus überein.

Аннотация—Для горизонтального течения воды и воздуха в кольцевом зазоре в трубе диаметром 1 дюйм проведены измерения перепада статического давления, а также локального и среднего коэффициентов теплообмена. Нагреваемая электричеством секция теплообменника из нерфавеющей стали длиной 60 дюймов была расположена приблизительно на расстоянии 105 дюймов по течению от места входа жидкости. Температура стенки трубы измерялась с помощью 57 термопар, заделанных в стенку, и 22 поверхностных термопар. Расход воды изменялся от 0,0714 до 0,3836 фунт/сек; а расход воздуха от 0,0300 до 0,2573 фунтов/сек; тепловой поток был равен 7372–12 772 бте/ч.фут^2. Значительные изменения температуры стенки по периметру трубы наблюдались при низких расходах воздуха. Полчена корреляция для коэффициентов теплообмена. Данные по перепаду давления согласуются с корреляцией Локхарта–Мартинелли и теорией Вробеля–Мак–Мануса.